National Aeronautics and Space Administration


# Commercial Sensor Survey
# Fiscal Year 2010
# Radiation Test Report

Heidi N. Becker
Dennis O. Thorbourn
James W. Alexander
Allan R. Eisenman

Jet Propulsion Laboratory
Pasadena, California

Jet Propulsion Laboratory
California Institute of Technology
Pasadena, California

JPL Publication 10-7 09/10

National Aeronautics and Space Administration


# Commercial Sensor Survey
# Fiscal Year 2010
# Radiation Test Report

NASA Electronic Parts and Packaging (NEPP) Program
Office of Safety and Mission Assurance

Heidi N. Becker
Dennis O. Thorbourn
James W. Alexander
Allan R. Eisenman

Jet Propulsion Laboratory
Pasadena, California

NASA WBS: 724297.40.49.11
JPL Project Number: 103982
Task Number: 03.04.02

Jet Propulsion Laboratory
4800 Oak Grove Drive
Pasadena, CA 91109
http://nepp.nasa.gov

This research was carried out at the Jet Propulsion Laboratory, California Institute of Technology, and was sponsored by the National Aeronautics and Space Administration Electronic Parts and Packaging (NEPP) Program.

**Table of Contents**

**Acronym List**

| | |
|---|---|
| ADC | Analog-to-Digital Converter |
| CCD | Charge-coupled device |
| CMOS | Complementary Metal Oxide Semiconductor |
| DDD | Displacement Damage Dose |
| DN | Digital Number (analog-to-digital converter count) |
| FPN | Fixed Pattern Noise |
| IFP | Image Flow Processor |
| LED | Light Emitting Diode |
| NEPP | NASA Electronic Parts and Packaging (Program) |
| RGB | Red-Green-Blue (filter) |
| RMS | Root Mean Squared |
| SOC | System-on-Chip |
| TID | Total Ionizing Dose |
| UC | University of California |

## 1.0 Introduction

The NASA Electronic Parts and Packaging (NEPP) Program Sensor Technology Commercial Sensor Survey task is geared toward benefiting future NASA space missions with low-cost, short-duty-cycle, visible-wavelength imaging needs. Such applications could include imaging for educational outreach purposes or short surveys of spacecraft, planetary, or lunar surfaces. Under the task, inexpensive, low-power, commercial grade CMOS sensors were surveyed in fiscal year 2007 (FY07), and three sensors were selected and tested for total ionizing dose (TID) and displacement damage dose (DDD) tolerance in fiscal year 2008 (FY08). The selected sensors had to meet selection criteria chosen to support small, low-mass cameras that produce good resolution color images. These criteria were discussed in detail in [1], and are provided again in Appendix 1 of this document. The commercial CMOS sensors tested under the task in FY08 showed very promising tolerance to TID and DDD levels typical of outreach and survey camera applications. The FY08 radiation test compendium produced by this task supported sensor selection for a recent space camera application.

In fiscal year 2009 (FY09), the survey was broadened to include two additional, similar sensor products. The fiscal year 2009 master compendium [2] provides results for all radiation testing performed on the Micron® and OmniVision sensors that were selected for radiation tolerance testing in FY08 and FY09.

This document presents results for an additional commercial CMOS sensor tested in FY10, the Aptina (formerly Micron®) MT9D131 CMOS Camera System-on-a-Chip.

## 2.0 Sensor Selected for Radiation Testing in FY10

In FY10, we continued to direct our sensor selection toward technologies that represent the current state-of-the-art for inexpensive commercial CMOS sensors. This was done in order to avoid technologies which might be nearing obsolescence in the commercial market and might soon be unavailable for future space applications. In addition, many recent advances in commercial sensor technology are potentially advantageous for small space camera implementation and integration, including improvements in sensitivity, and the inclusion of on-chip image processing and data compression functionalities. Following are descriptions of the Aptina sensor selected for testing in FY10 and the manufacturer-supplied evaluation kit used for our characterizations. However, details of evaluation kit support software are proprietary to Aptina so they are not discussed in this document.

Several other commercial sensor manufacturers were surveyed for products meeting our selection criteria; however, additional viable candidates were not identified as of Spring 2010. This was due either to cost, the absence of a supporting evaluation kit, or because product availability did not meet task schedule requirements.

### 2.1 Aptina (Micron®) MT9D131C12STC (2 Mpixel, 1/3.2 inch, 2.8 µm) System-on-a-Chip (SOC)

The MT9D131 is a 2-Mpixel, 1/3.2-inch optical format, electronic rolling shutter (progressive scan) CMOS image sensor that includes the electronics for an integrated, advanced camera system on the chip. It has a 1600(H) × 1200(V) color pixel array with a red-green-blue (RGB) Bayer pattern color filter; the pixel size is 2.8 µm × 2.8 µm. Micron® Digital Clarity® CMOS imaging technology is used. Advertised low light responsivity is 1.0V/lux-sec (at 550nm). Power consumption is 348mW when imaging at

full resolution and 15 frames per second. The MT9D131 is marketed for security camera applications.

This SOC includes two 10-bit analog-digital converters (ADCs), an image flow processor (IFP), a microcontroller, and a real-time JPEG encoder. Among the automatic image control functions are automatic exposure control, automatic black level offset correction, automatic white balance, lens shading, flicker avoidance, color saturation control, and defect identification and correction. Selectable output formats are ITU-R BT.601 (YCbCr), 565RGB, 555RGB, 444RGB, JPEG 4:2:2, JPEG 4:2:0, and Raw 10-bit. A functional block diagram of the MT9D131 is shown in Figure 1.

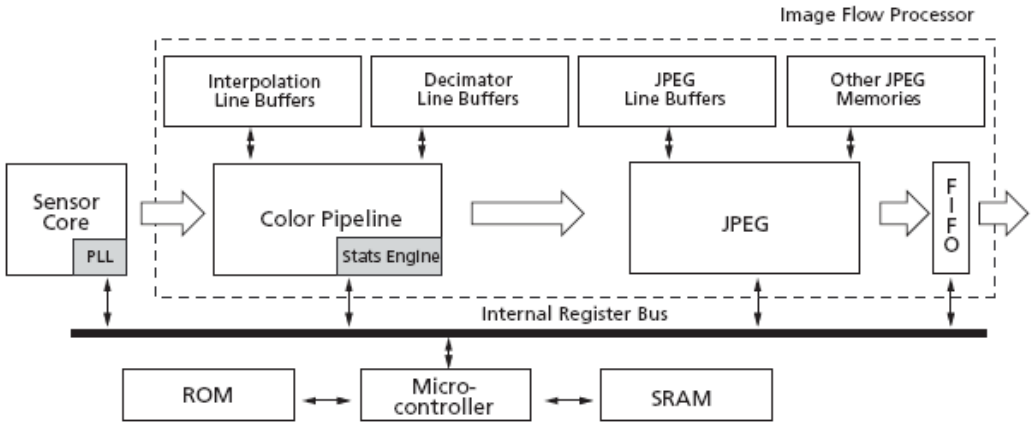


**Fig. 1.** MT9D131 Functional Block Diagram [3]

## 2.2 Aptina Evaluation Kit

Evaluation of the MT9D131 was supported by the Aptina MT9D131C12STCD ES Demo Kit. The MT9D131C12STCD ES is a digital evaluation kit with a detachable image sensor headboard that contains a solder-mounted MT9D131 sensor sample and removable optics (Figures 2–4) [4]. The headboard design allows test sensor samples to be irradiated without removing them from the image sensor headboards or harming any support electronics (optics were removed and proximity support electronics were shielded during irradiation). Test samples for the MT9D131 were procured as individual image sensor headboards.

**Fig. 2.** MT9D131C12STCD ES Demo Kit


**Fig. 3.** MT9D131 Image Sensor Headboard


**Fig. 4.** MT9D131 Image Sensor Headboard with Lens Barrel Removed

## 3.0 Test Bench

### 3.1 Sensor Characterization Test Bench

The Commercial Sensor Survey test bench (Figure 5) has a shrouded black box that can be used for collecting dark frames or imaging. Internal equipment includes a neutral white LED light source and an integrating sphere for flat field illumination, neutral density filters, a color bar target for imaging, and thermocouples for monitoring ambient temperature and sensor proximity board temperature. Sensor register settings and data collection are controlled via a laptop interface. This test bench was used for all pre- and post-irradiation characterizations.

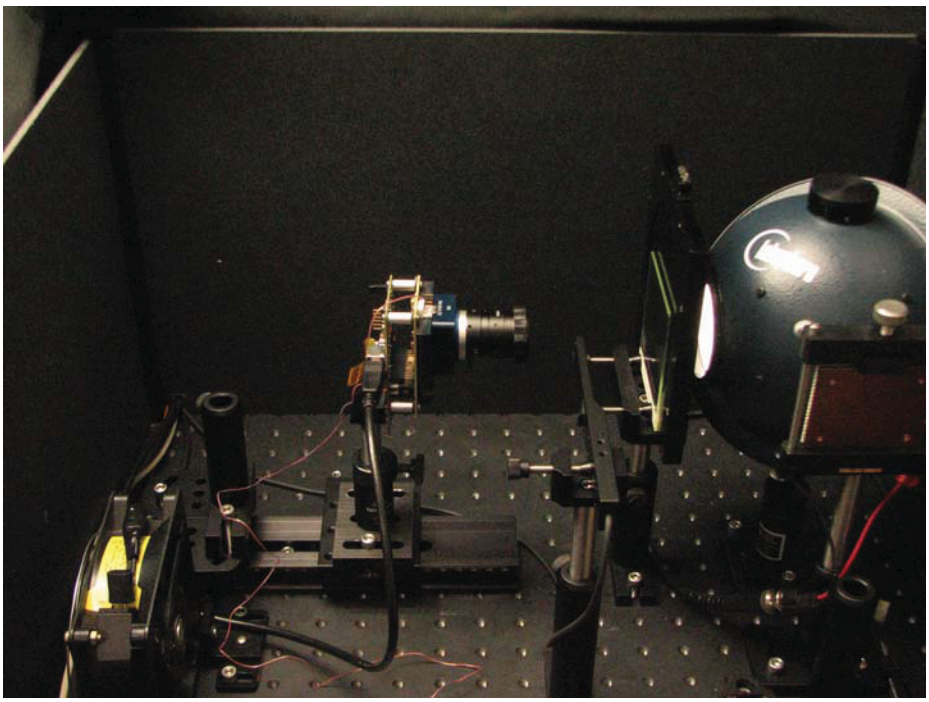

**Fig. 5.** Commercial Sensor Survey Test Bench

### 3.2 Co-60 Irradiation Configuration

During Co-60 irradiations, test samples were powered in a video data mode, but data were not collected during irradiation. A shielded support computer was positioned in the irradiation cell to opperate the sample under test. A 6-sided lead bunker was used to provide shielding for all camera support electronics (Figures 6 and 7). The side of the bunker facing the Co-60 source was a custom lead shield, containing a small aperture that allowed only the sensor sample under test to be exposed. A lead/aluminum plate was installed in front of the test sample during the irradiations, per MIL STD 883, method 1019.

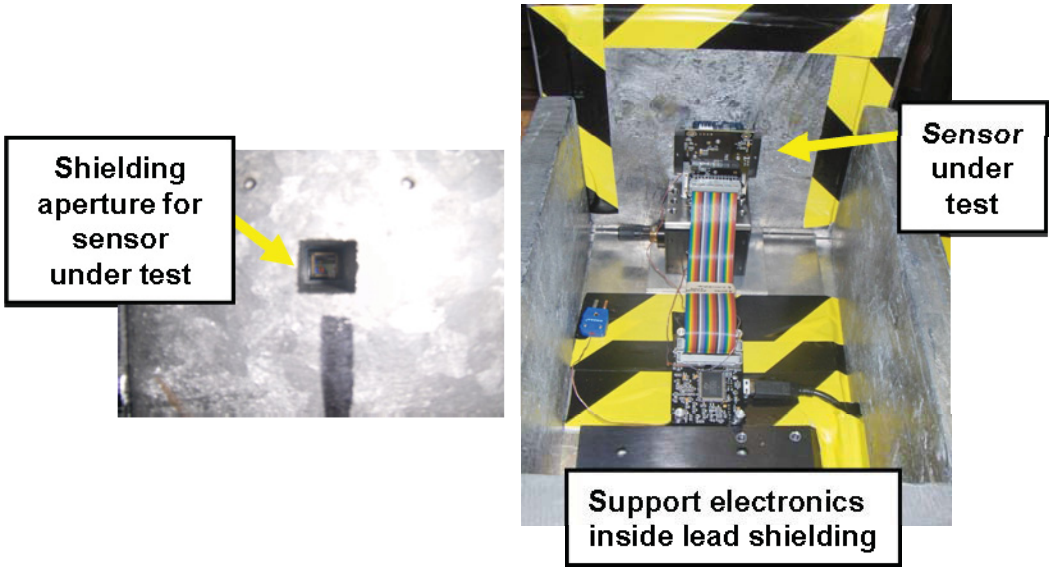


**Fig. 6.** Lead Shielding Used for Co-60 Irradiations

**Fig. 7.** Shrouded Lead Bunker in Front of Co-60 Source

## 4.0 Characterization Approach

### 4.1 Characterization Protocols

As in FY09, the relative complexity of the on-chip functions and IFP algorithms of the MT9D131 made it impossible to operate our test samples in a purely manual mode without some internal signal adjustment taking place (e.g. black level conditioning). Due to our lack of visibility on several proprietary aspects of internal sensor functions, we chose to focus our characterizations on parameters and image characteristics where the impact of our selected register settings was clear. Our focus was placed on control of exposure time, gain, and image processing functions, with special emphasis on defective pixel correction. Our protocols observed the following general approaches:

1) Data collection with sensor register settings adjusted to control parameters that can influence characterization results:

    a) Use of fixed exposure times and fixed internal gains (combination of analog and digital gains) to ensure integrity of all pixel data without pixel or ADC saturation
    b) Disabled on-chip image correction features where possible (some, such as black level conditioning, could not be disabled) for determination of dark signal and pixel noise

2) Data collection in an 8-bit processed image format with the defect correction algorithm enabled, versus disabled, to observe how radiation degradation effects (especially proton-induced “hot pixels”) are corrected internally by the sensor

3) Data collection using default evaluation kit auto settings for qualitative color image assessment

Note that in a camera application, the camera designer would likely choose some combination of manually controlled and auto-controlled register settings, depending on the particular imaging need and the facility to program these parameters.

### 4.2 Data Sets

The following types of data were collected pre- and post-irradiation:

1) Dark frames collected at fixed integration times (used for pixel dark signal and pixel noise assessments).

    a) 8-bit processed format with defect correction OFF
    b) 8-bit processed format with defect correction ON

2) Color bar target images taken at best focus for qualitative imaging assessments.

    a) Default evaluation kit auto settings; 8-bit processed format
    b) Verification that defect correction function was enabled

3) Prior to irradiation, flat field images were also collected at several different integration times in a 10-bit format (used for photon transfer curves).

Each data set included multiple frames that were taken under identical conditions in rapid succession. Dark, flat field, and image frame data sets included 5–6 frames. Optically "black" (light-shielded) pixel values, used to provide data for on-chip offset correction algorithms (black level control) [3], were not available as output using the 8-bit processed format. All data were collected at ambient temperature.

### 4.3 Analyzed Sensor Parameters and Characteristics

Gain: CMOS sensor (camera) gain in signal electrons/ADC unit (e/DN)

Spatial Pixel Signal Distributions (Dark Signal): The distribution of pixel signal values under un-illuminated conditions

Fixed Pattern Noise: The spatial standard deviation pixel value for a given color channel. The calculations in this report were performed using data taken under un-illuminated conditions.

Mean Pixel (Dark) Signal: The average pixel signal for a given color channel, calculated using data collected under un-illuminated conditions

Pixel Noise: The standard deviation signal value for each pixel location. RMS pixel noise was calculated over all pixel locations for a given color channel. The calculations in this report were performed using data taken under un-illuminated conditions. Pixel noise under these conditions includes a combination of thermal dark current shot noise, output amplifier noise, on-chip electronic noise, and any uncorrected offset noise or pixel reset noise.

Defective Pixel Canceling: Comparison of pixel dark signal distributions, pixel noise, and mean pixel signals for dark frames collected with and without the defect correction function enabled

Qualitative image comparisons: Assessment of image quality pre- and post-irradiation

*Representative parametric characterization results are shown for the red color channel in this report. Results for the red, blue, and green color channels were similar.*

## 5.0 Radiation Test Levels

In FY08/09 our radiation test levels were based on a range of displacement damage dose (DDD) and total ionizing dose (TID) levels that are considered typical for outreach or survey cameras in Earth orbit or Deep Space solar flare environments (e.g., Mars); TID levels ranged from 500 rad(Si) to 5 krad(Si). Such cameras typically have to compete with other payloads and flight system instruments, which may have higher priority for available shielding mass and strategic positioning on the spacecraft. Therefore, the negotiated amount of shielding would depend on the priority of the camera's data return, how early in the mission the camera would be expected to achieve its requirements, the relative radiation sensitivity of the sensor technology, and the risk to meeting performance requirements due to radiation degradation or transient noise.

In FY10 we added additional higher cumulative TID levels of 10 and 20 krad(Si) because the good performance we observed after the 5 krad(Si) level in earlier years encouraged us to extend the testing. Irradiation was also extended to a cumulative TID level of 30 krad(Si) on one sample.

In the environments considered, high energy protons are the dominant contributors to cumulative mission DDD and TID. 50-MeV protons were selected for our irradiations because this energy is representative of the typical radiation spectrum at the detector level, after having passed through instrument shielding. This allowed us to perform representative TID and DDD testing simultaneously. The radiation test levels listed in Table 1 show target TID levels and the corresponding 50-MeV proton test fluence and DDD in silicon.

**Table 1.** FY10 Radiation Test Levels

| Total Ionizing Dose (TID) krad(Si) | 50-MeV† Proton Test Fluence (protons/cm$^2$) | Displacement Damage Dose (MeV/g)* |
|---|---|---|
| 2 | 1.26E10 | 4.9E7 |
| 5 | 3.16E10 | 1.2E8 |
| 10 | 6.32E10 | 2.5E8 |
| 20 | 1.26E11 | 4.9E8 |
| 30 | N/A (level used for Co-60 testing) | N/A (level used for Co-60 testing) |

*DDD was calculated using the following relationship:

**DDD (MeV/g) = test particle NIEL (MeV·cm$^2$/g) × test particle fluence (particles/cm$^2$)**

[calculations performed using 3.884E-3 MeV*cm$^2$/g Si(21eV) NIEL value for 50-MeV protons from Summers et. al, *IEEE Trans. Nucl. Sci*., 40(6), Dec. 1993]

†It was not possible to procure our test samples with removable cover glass, so irradiations had to be performed through the sensor cover glass. Proton energy loss calculations for incident 51-MeV protons (used for all irradiations) were performed using manufacturer-supplied information on cover glass thickness and material. The energy loss was ~1-MeV, and the proton energy incident on the sensor die was 50-MeV.

TID testing was performed at the Jet Propulsion Laboratory's (JPL's) Co-60 ionizing dose facility in July/August 2010, and combined TID/DDD testing was performed with 50-MeV protons at the University of California (UC) Davis cyclotron in June 2010.

Our sample sizes were constrained due to irradiation facility availability. Three samples were irradiated during Co-60 testing. Two of these samples were powered during irradiation (sensor response was similar for these two samples) and one was unpowered during irradiation. Each sample was incrementally irradiated and characterized after exposure to cumulative total ionizing doses of 2 krad(Si), 5 krad(Si), 10 krad(Si), and 20 krad(Si). Testing on one of the powered samples was extended to 30 krad(Si) (Figure 8).

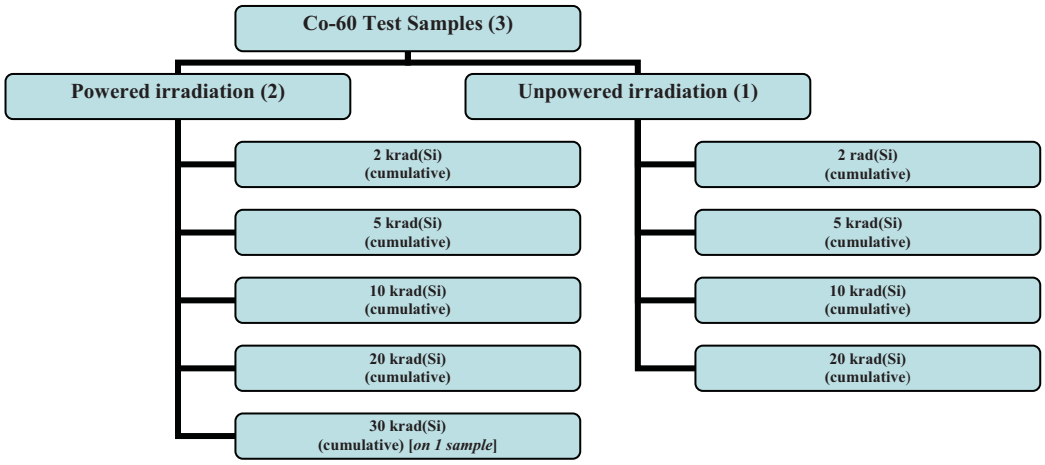


**Fig. 8.** Co-60 Radiation Test Sample Allocation

During proton testing, one sample was irradiated to each of the levels shown in Figure 9 and returned to JPL for characterization; no incremental dose testing or on-site characterization at UC Davis was performed.

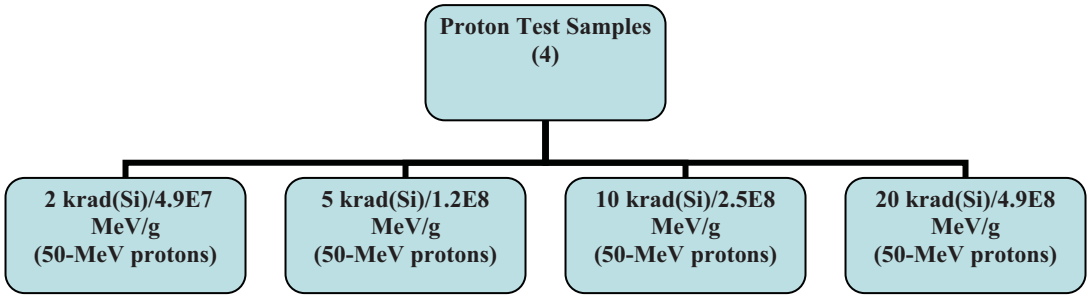


**Fig. 9.** 50-MeV Proton Radiation Test Sample Allocation

## 6.0 Radiation Test Conditions

Proton test samples were irradiated unpowered with all leads shorted to ground. Unpowered irradiation was chosen for proton testing because it is considered representative of the low-duty cycles of the camera applications addressed by this study. Initial characterizations were performed within several days following irradiation. Characterizations were repeated and augmented 7 weeks following irradiation to include improved characterization of the MT9D131 automatic defect correction function's ability to mitigate hot pixels.

Co-60 irradiations were performed with samples powered in the evaluation kit's default video mode for two of the three Co-60 samples. This test condition was considered more conservative (worst case) than an unpowered irradiation, as CMOS technologies often experience a larger degree of degradation when ionizing dose is applied under a powered condition [5]. A 10 rad(Si)/s dose rate was used. Following irradiation to each target TID increment, samples were removed from the irradiation camera support circuitry and transferred to the characterization test bench for post-irradiation characterization. Characterizations were completed within 1 to 2.5 hours following each incremental TID exposure. A third Co-60 sample was irradiated unpowered with all leads shorted to ground because the SOC degradation observed under powered Co-60 irradiation was significantly more severe than that observed following proton irradiation.

## 7.0 FY10 Test Results

### 7.1 Bar Target Images (Default Evaluation Kit Auto Settings)

Figure 10 shows several color bar target images taken with the MT9D131, using default evaluation kit settings and enabled automatic IFP functions. Performance is qualitatively similar before irradiation and after irradiation up to 10 krad(Si) with 50-MeV protons. An increasing number of "hot pixels" are unmitigated by the defect correction algorithm as the test level increases. The defect correction algorithm replaces the actual values of identified "defective" pixels with values inferred from the values of same-color nearest neighbor pixels [3]. At higher proton fluences a denser population of "hot" same-color nearest neighbor pixels may contribute to the reduced effectiveness of the defect correction

algorithm. At 20 krad(Si) imaging quality and SOC functionality is noticeably impacted under the imaging register settings selected under the default evaluation kit mode.

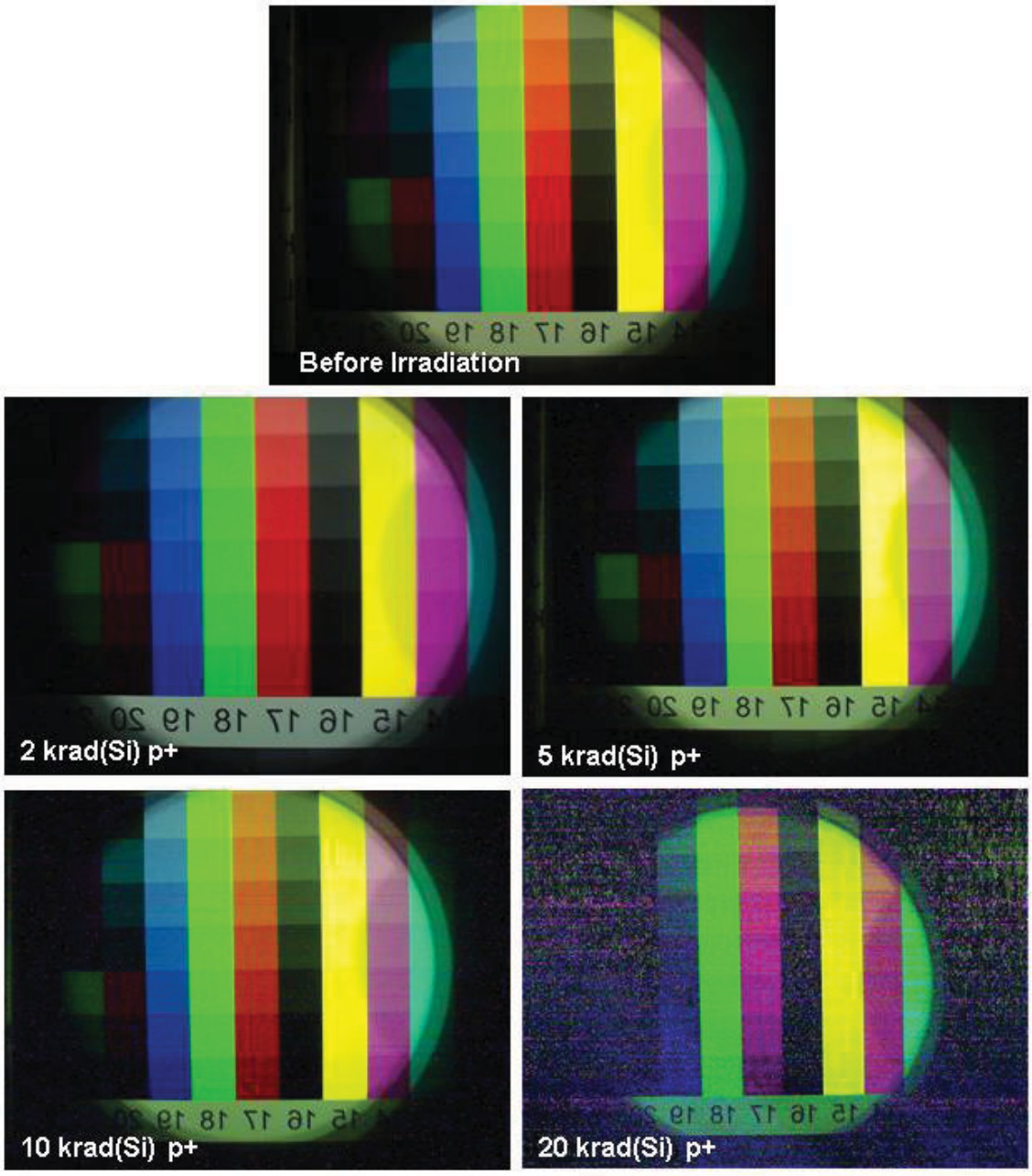


**Fig. 10.** Color bar target images taken with default MT9D131 settings and enabled automatic IFP functions following proton irradiation. Imaging performance is qualitatively similar prior to irradiation and after irradiation up to 10 krad(Si) with 50-MeV protons, although higher numbers of unmitigated hot pixels are seen as the test level increases. At 20 krad(Si) imaging quality and SOC functionality is noticeably impacted under default evaluation kit register settings.

Imaging quality and SOC functionality under default evaluation kit register settings were highly degraded following powered irradiation to 20 krad(Si) with Co-60. This degradation was much more severe than that seen at 20 krad(Si) for unpowered irradiations with 50-MeV protons or Co-60. Figure 11 compares color bar target images taken with default MT9D131 evaluation kit register settings for three different samples irradiated to 20 krad(Si) under different irradiation test conditions. An image collected following extended irradiation to 30 krad(Si) on a powered Co-60 sample is also shown; the functional loss at 30 krad(Si) was qualitatively similar to that seen at the 20 krad(Si) level. More degradation at 20 krad(Si) is seen in the unpowered sample irradiated with 50-MeV protons than in the unpowered Co-60 sample, which may be due to the additional impact of proton-induced displacement damage in the proton irradiated sample.

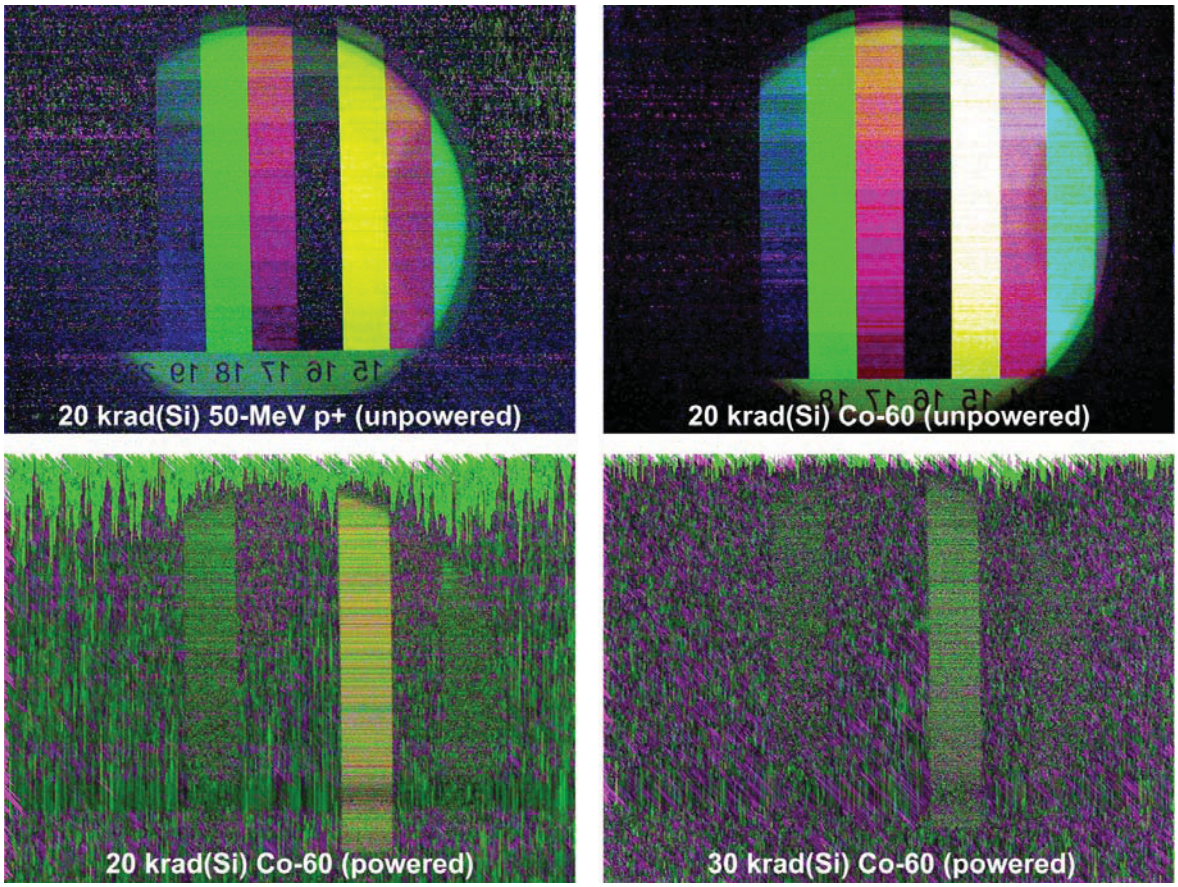


**Fig. 11.** Color bar target images taken with default MT9D131 register settings and enabled automatic IFP functions. At 20 krad(Si) imaging quality and SOC functionality under default evaluation kit register settings is significantly more degraded under powered irradiation conditions.

Noticeable degradation was also present at 10 krad(Si) under powered Co-60 irradiation (unpowered test samples showed relatively minor degradation at 10 krad(Si)). Figure 12 illustrates the greater degradation in imaging quality seen at 10 krad(Si) when Co-60 irradiation was performed under a powered condition. The unpowered sample continued to show good qualitative imaging performance under default evaluation kit register settings at this level.

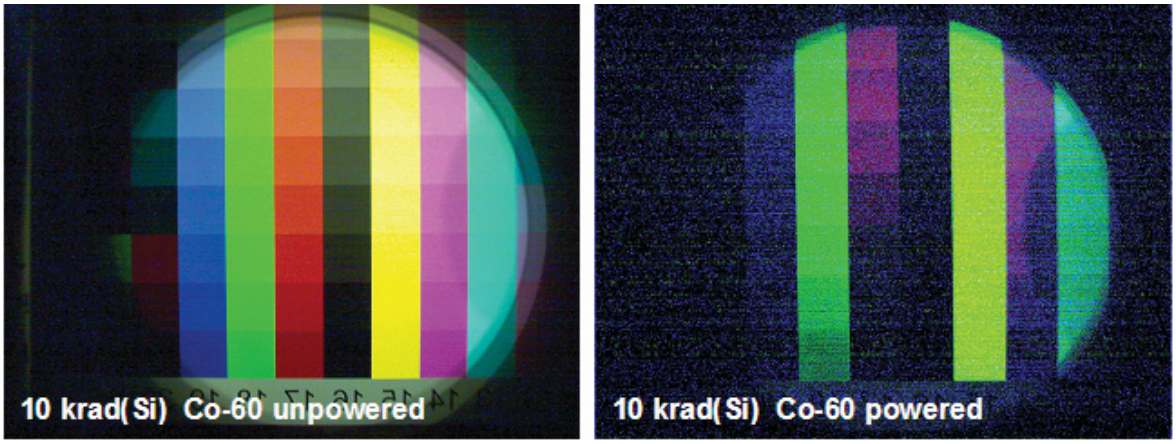


**Fig. 12.** Color bar target images taken after Co-60 irradiation to 10 krad(Si) with default MT9D131 register settings and enabled automatic IFP functions. The unpowered sample shows relatively minor degradation in imaging performance compared to the powered sample.

## 7.2 Parametric Characterizations

### 7.2.1 Gain

Data in this report are expressed in terms of digital number (DN; analog-to-digital converter count). The conversion from DN to electrons was calculated by plotting the signal variance ($DN^2$) vs. average signal level under flat field illumination conditions. For the range of signal levels dominated by shot noise, electron gain is given by the slope of this linear region [6]:

$$\text{e/DN} = \frac{\overline{signal}(DN)}{\sigma^2(DN^2)} \qquad (1)$$

Calculated electronic gain (e/DN) for the MT9D131 is shown in the photon transfer curve in Figure 13 and Table 2. Red pixel data from 5 full resolution frames were collected under diffused red LED illumination and used in the photon transfer curve calculations.

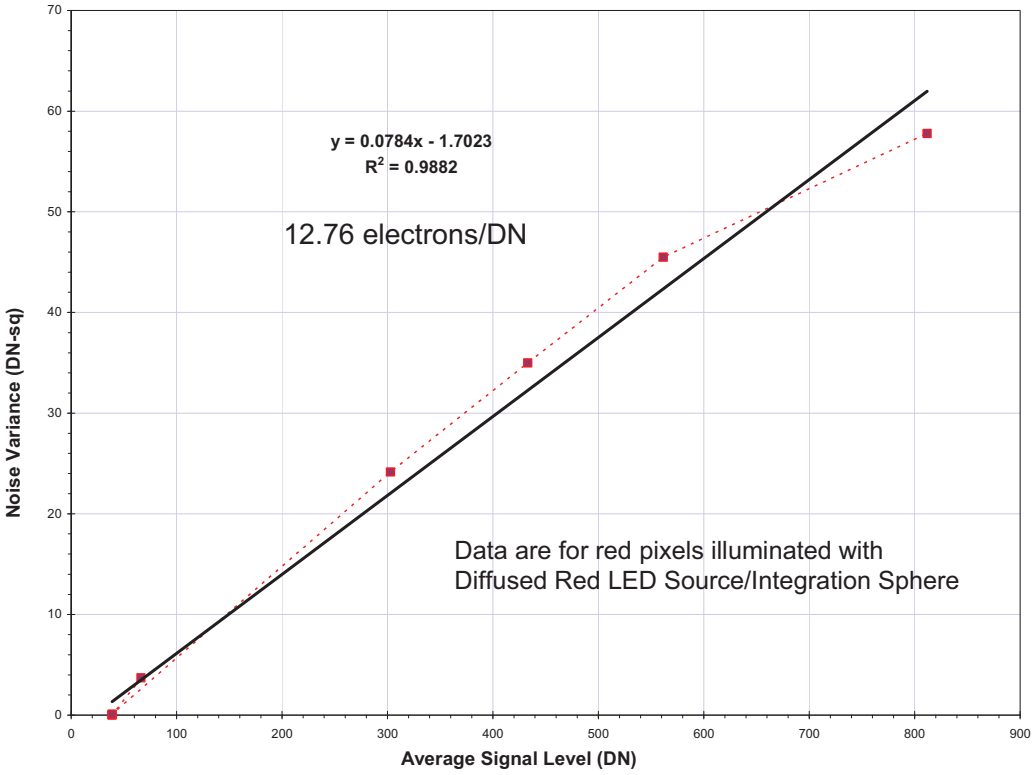


**Fig. 13.** Photon Transfer Curve for an Unirradiated MT9D131 Sample

**Table 2.** Calculated Electronic Gain (e/DN)

| Sensor | MT9D131 |
|---|---|
| electrons/DN | 12.8 |
| # of DN full-scale | 1024 |

### 7.2.2 Pixel Defect Correction

The integrated image flow processor (IFP) of the MT9D131 performs "on-the fly" defect correction to mitigate pixel array defects such as damaged or high dark signal rate "hot pixels" [3]. In order to isolate and assess the effect of the on-chip defect correction algorithm, dark frame data were collected with this function enabled ("ON") or disabled ("OFF"), under otherwise similar conditions. Other IFP functions were disabled where possible; recall that it was not possible for us to disable the black level subtraction processing function of the MT9D131. The spatial pixel signal distributions of these frames can be compared to highlight defective pixel corrections. In the following frame comparisons, all data were collected using a 100 ms exposure time and a gain of 1. Pixels from the red RGB color channel are shown.

The benefit of the defect correction function is particularly evident following proton irradiation. The numbers of higher dark signal pixels in the "tails" of the distributions are noticeably reduced by enabling defect correction. Enabled defect correction also reduces higher signal pixel values in the powered and unpowered Co-60 data, but there are much fewer pixel defects to mitigate following Co-60 irradiation due to the relatively small presence of displacement damage. Figures 14–17 compare pixel signal distributions for

single dark frames collected with defect correction functions ON and OFF following irradiation to 2, 5, 10, and 20 krad(Si), respectively. In each of these figures pixel distributions for unpowered proton, unpowered Co-60, and powered Co-60 samples are shown. Figure 18 shows pixel signal distributions for the powered Co-60 sample which was irradiated to 30 krad(Si).

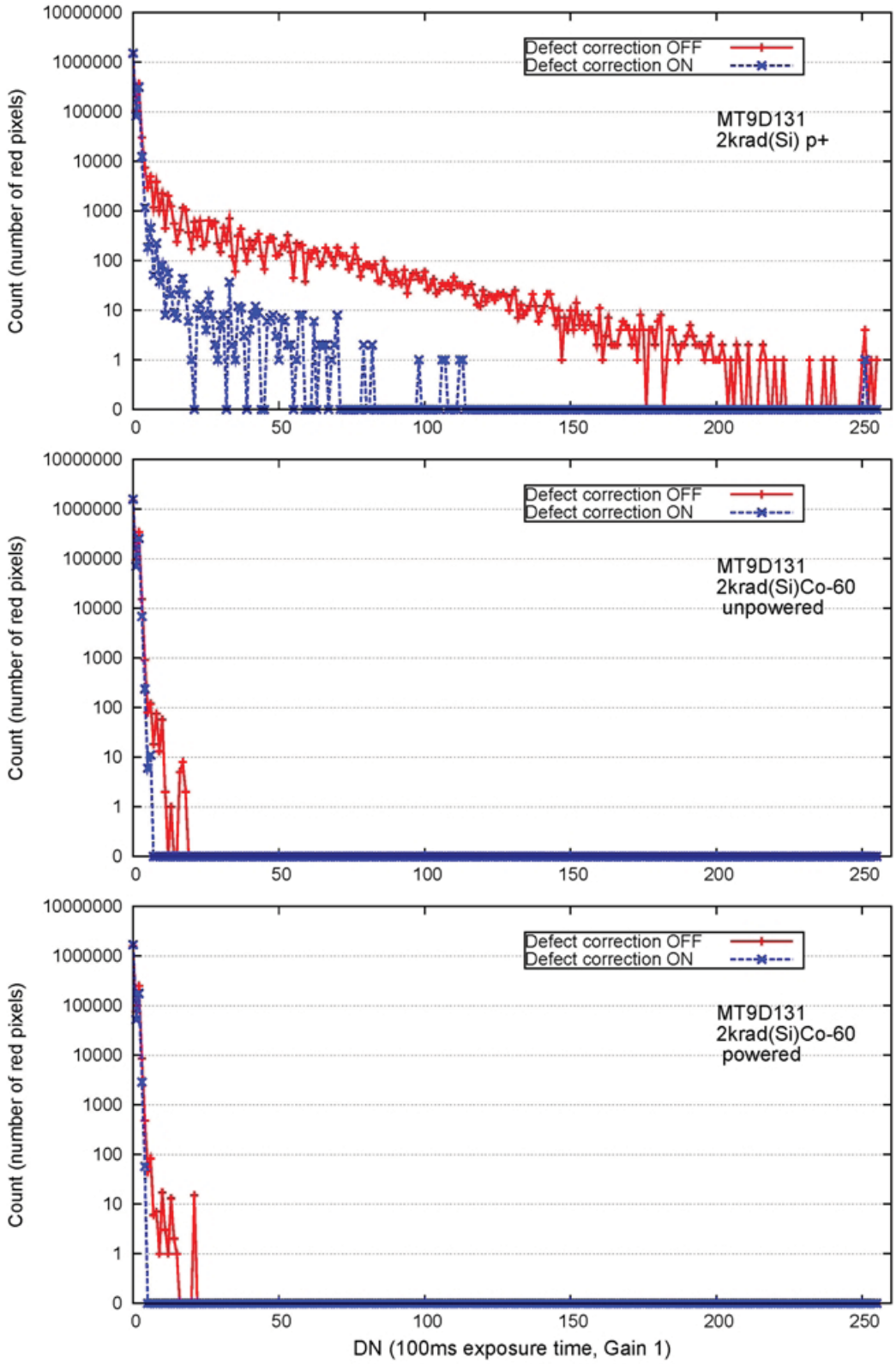


**Fig. 14.** MT9D131 spatial pixel signal distributions for dark frames collected with defective pixel canceling functions ON and OFF following irradiation to 2 krad(Si).

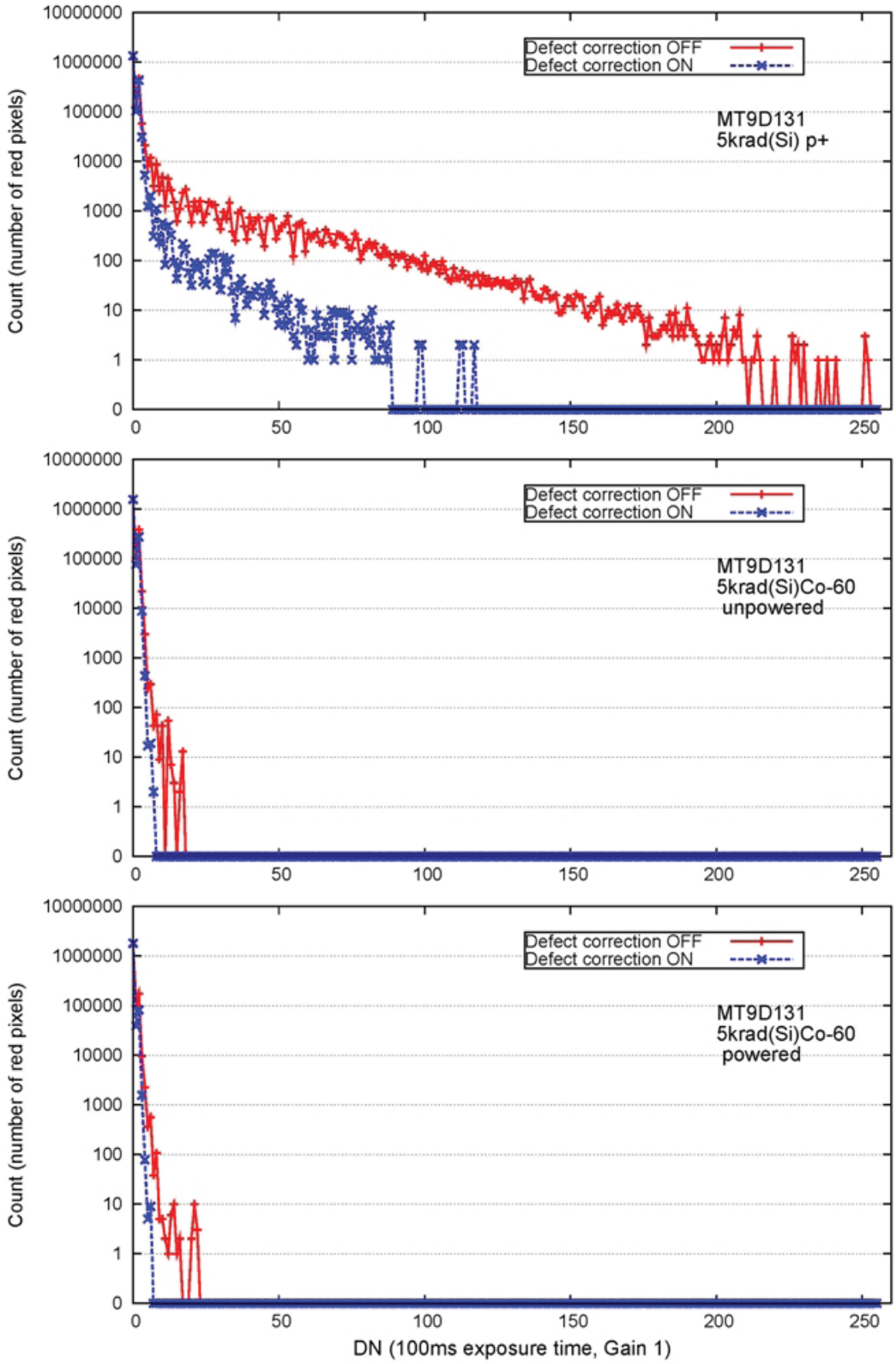


**Fig. 15.** MT9D131 spatial pixel signal distributions for dark frames collected with defective pixel canceling functions ON and OFF following irradiation to 5 krad(Si).

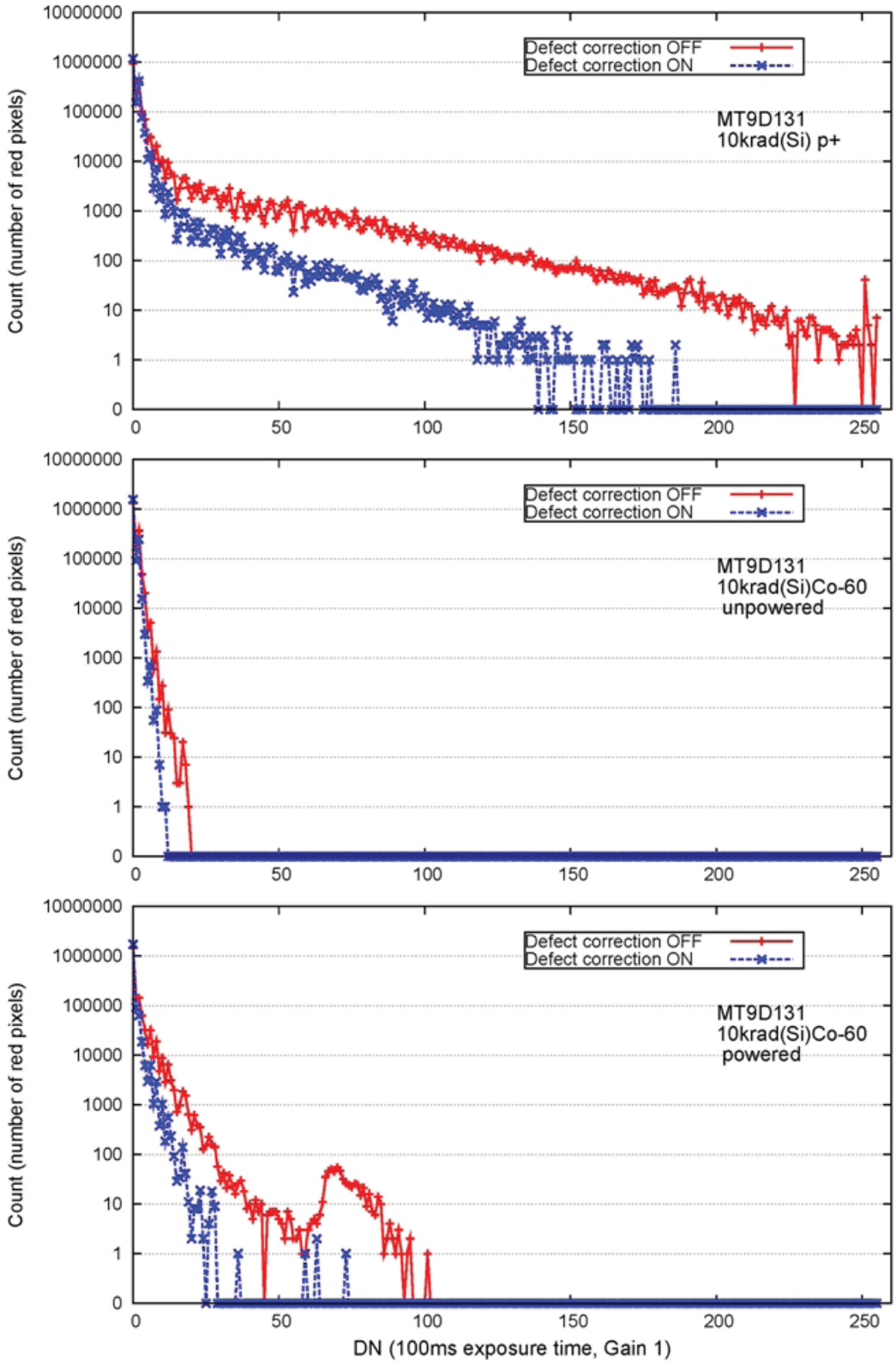


**Fig. 16.** MT9D131 spatial pixel signal distributions for dark frames collected with defective pixel canceling functions ON and OFF following irradiation to 10 krad(Si).

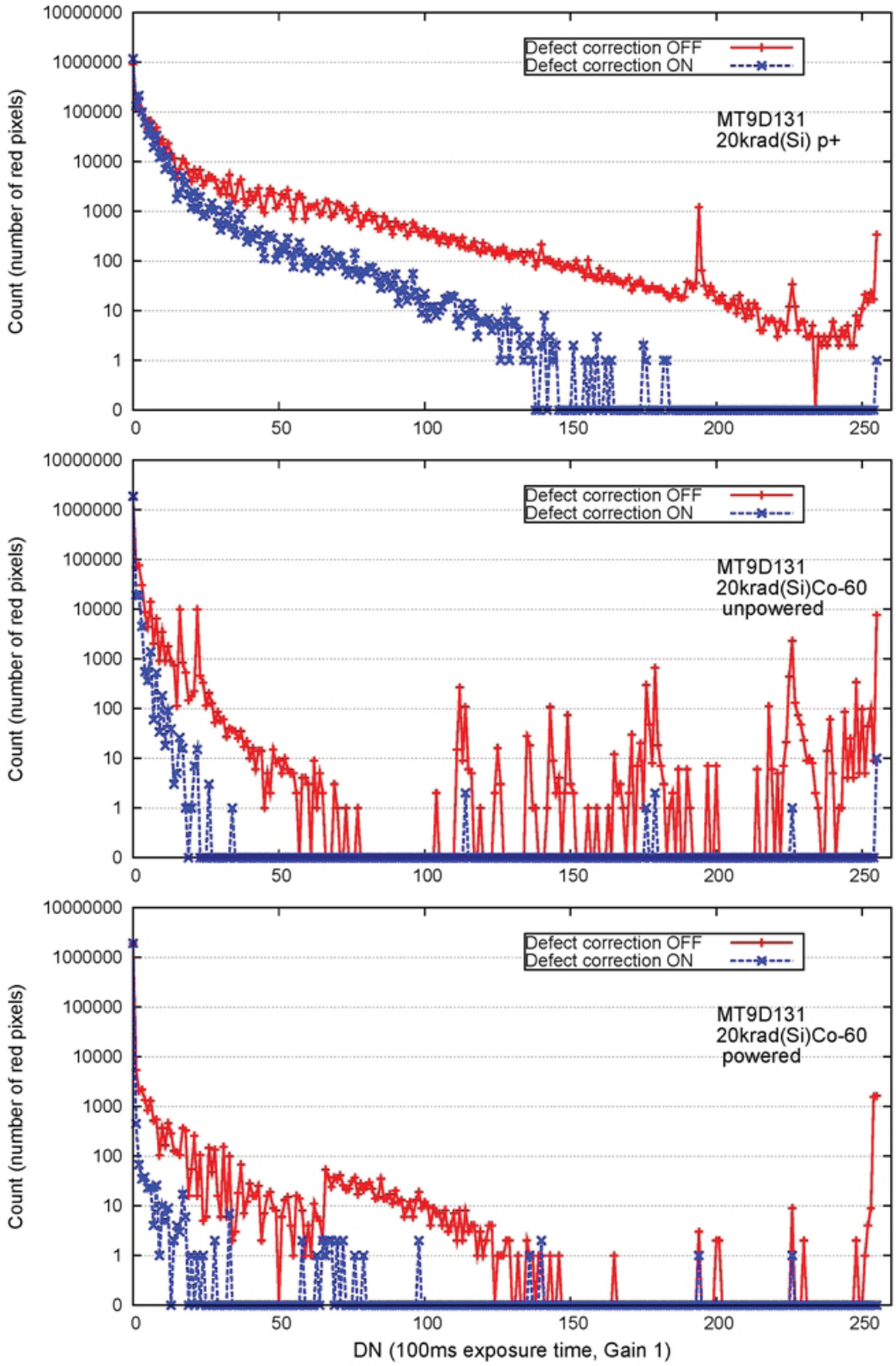


**Fig. 17.** MT9D131 spatial pixel signal distributions for dark frames collected with defective pixel canceling functions ON and OFF following irradiation to 20 krad(Si).

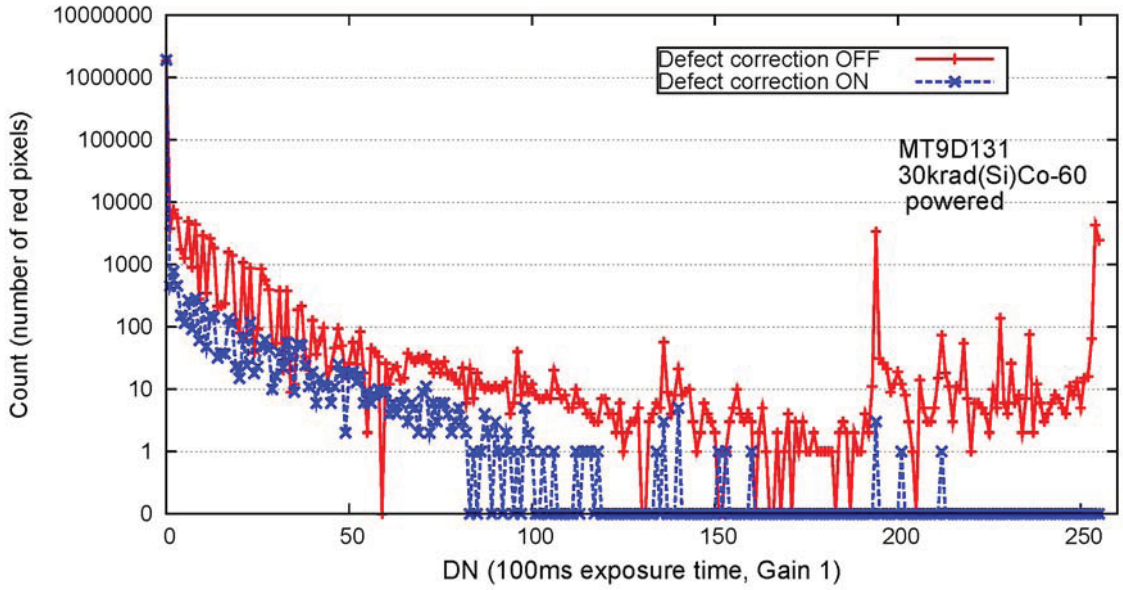


**Fig. 18.** MT9D131 spatial pixel signal distributions for dark frames collected with defective pixel canceling functions ON and OFF following powered irradiation with Co-60 to 30 krad(Si).

Table 3 lists calculated fixed pattern noise (FPN) for the radiation levels and conditions shown in Figures 14–18. Pre-irradiation FPN is also shown. The FPN calculations were performed using average red pixel position values calculated over 5 dark frames. The reduction in FPN from enabling the defect correction algorithm can be seen, and is most significant in the proton data. Note that there is not a clear trend in the Co-60 FPN data to indicate whether powered or unpowered irradiation is more degrading to the MT9D131. At 10 krad(Si) FPN is worse in the powered Co-60 sample, but at 20 krad(Si) FPN is worse in the unpowered one. This is an example, as noted in our FY09 compendium [2], where absolute parametric characterization of a SOC becomes challenging; it is not possible to disable the effects of black level conditioning processing or fully isolate pixel response from SOC functional degradation outside of the sensor core.

**Table 3.** Fixed Pattern Noise calculated for the red RGB color channel using five MT9D131 dark frames collected with 100ms exposure time and Gain 1.

| Test Level | FPN (DN) Protons DC OFF | FPN (DN) Protons DC ON | FPN (DN) Co-60 (Powered) DC OFF | FPN (DN) Co-60 (Powered) DC ON | FPN (DN) Co-60 (Unpowered) DC OFF | FPN (DN) Co-60 (Unpowered) DC ON |
|---|---|---|---|---|---|---|
| Before irradiation | 0.423 | 0.36 | 0.414 | 0.339 | 0.44 | 0.377 |
| 2 krad(Si) | 5.465 | 0.733 | 0.409 | 0.336 | 0.463 | 0.385 |
| 5 krad(Si) | 8.086 | 1.346 | 0.495 | 0.251 | 0.525 | 0.409 |
| 10 krad(Si) | 14.258 | 3.631 | **2.516** | 0.798 | **0.844** | 0.504 |
| 20 krad(Si) | 16.106 | 5.319 | **9.73** | 0.319 | **16.177** | 0.708 |
| 30 krad(Si) | n/a | n/a | 17.949 | 1.15 | n/a | n/a |

### 7.2.3 Mean Pixel (Dark) Signal

Autonomous black level conditioning processing is also likely influencing mean dark signal trends. Increases in mean pixel signal would be expected to be proportional to increases in exposure time, but this is not seen in our data.

Figure 19 compares mean red pixel signal values of proton irradiated samples for two different integration times. A similar comparison is shown in Figure 20 for unpowered and powered Co-60 samples. Note that under longer exposure times (1000ms and 2100ms) mean red pixel values in the powered Co-60 sample approach saturation at 10 krad(Si) when defect correction is OFF, but then *decrease* at higher levels of TID. This may be the result of black level conditioning given an increased number of damaged reference pixels.

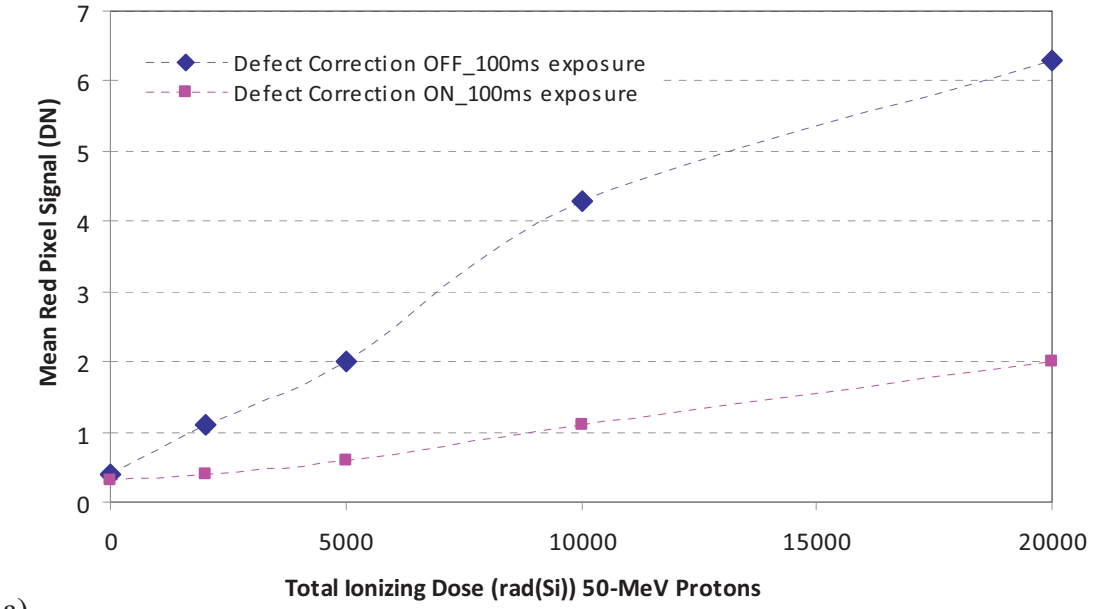


a)

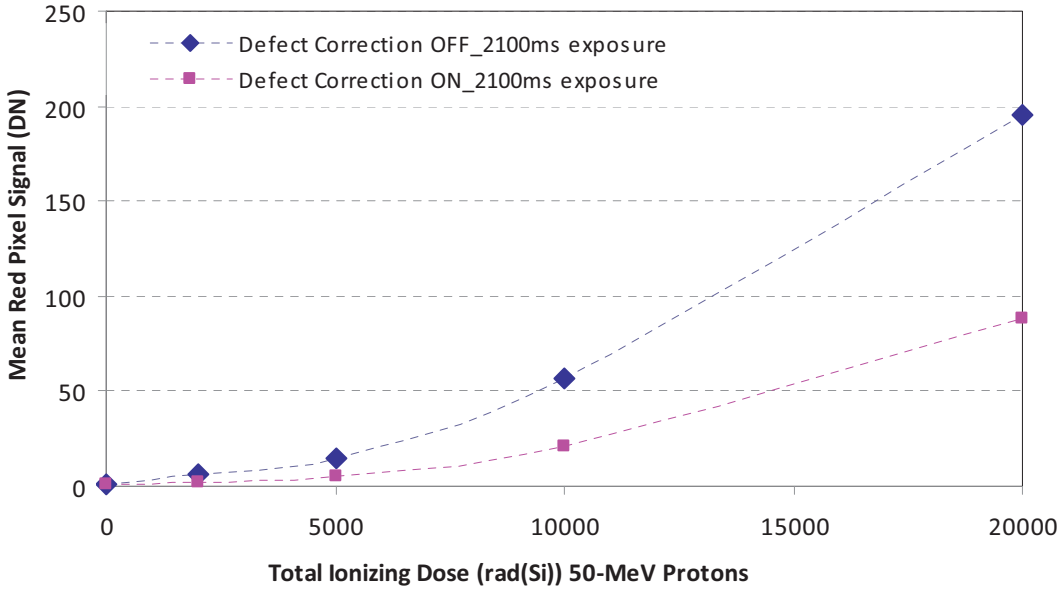


b)

**Fig. 19.** Mean red pixel signal following proton irradiation for exposure times of a) 100ms and b) 2100ms; Gain 1.

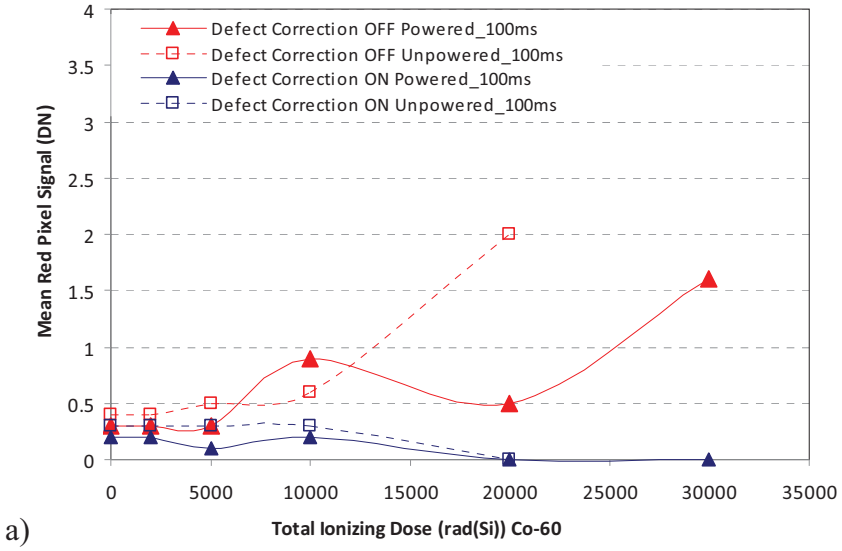


a)

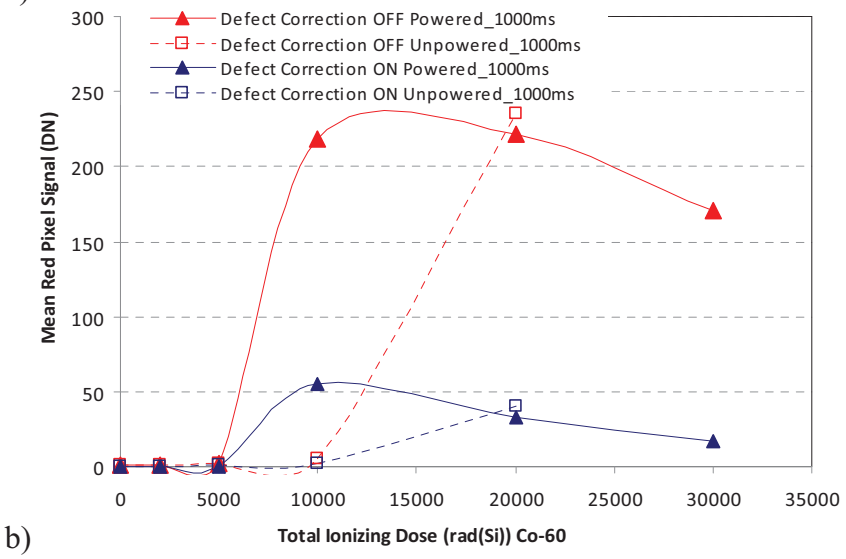


b)

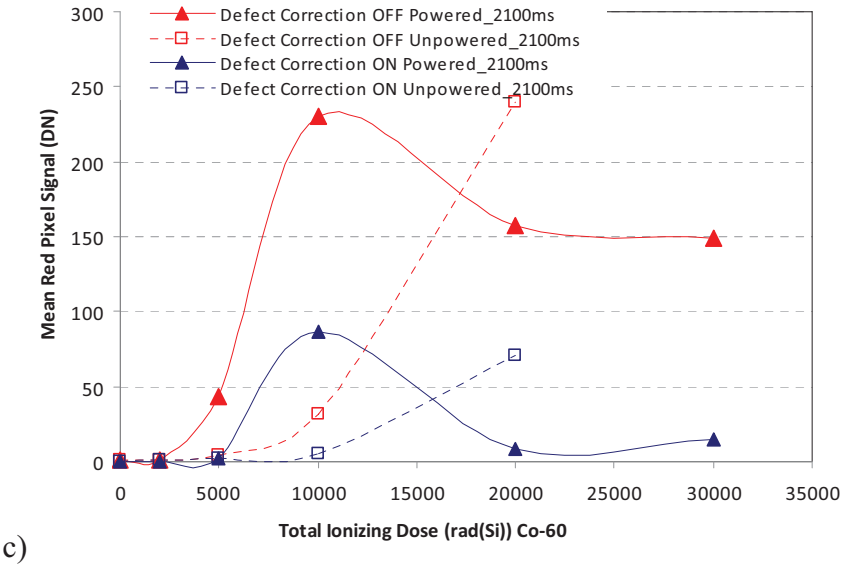


c)

**Fig. 20.** Mean red pixel signal following Co-60 irradiation for exposure times of a) 100ms, b) 1000ms, and c) 2100ms; Gain 1.

### 7.2.4 Pixel Noise

Pixel noise was calculated from dark frame data. Five dark frames were collected at each test level with the majority of IFP functions disabled (recall, black level conditioning could never be disabled). For each data set, noise was calculated at each red pixel position using the five values available from the given data set. RMS pixel noise (temporal noise) for red pixels was calculated from these values. Behavior was similar in the other RGB color channels.

Temporal noise for red pixels is shown in Figure 21 for proton-irradiated samples. For 100ms exposures the noise remains less than 1 DN to 5 krad(Si) and is still under 3 DN at 20 krad(Si). Noise at longer exposures of 1000ms and 2100ms was greater than at 100ms for the proton samples irradiated to higher levels (5, 10, or 20 krad(Si)). However, the noise increases did not scale with the increases in exposure time nor were they completely consistent with increasing radiation levels.

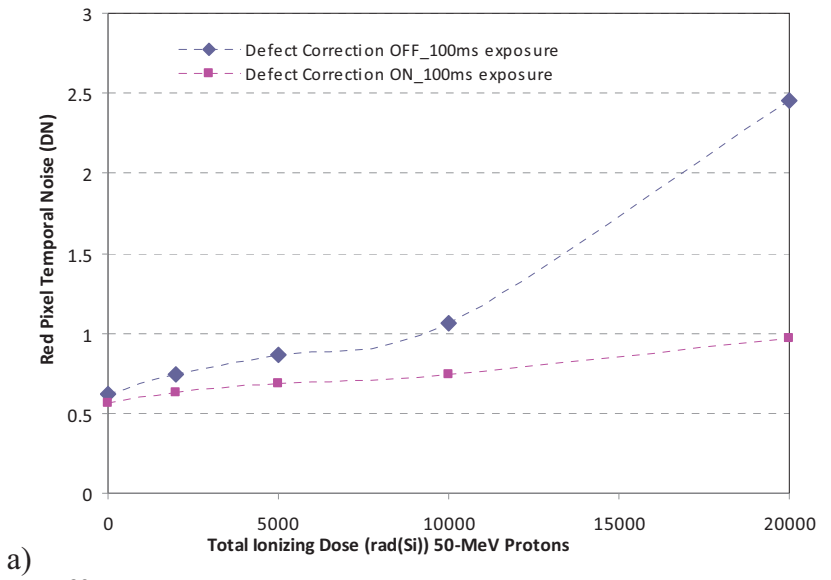


a)

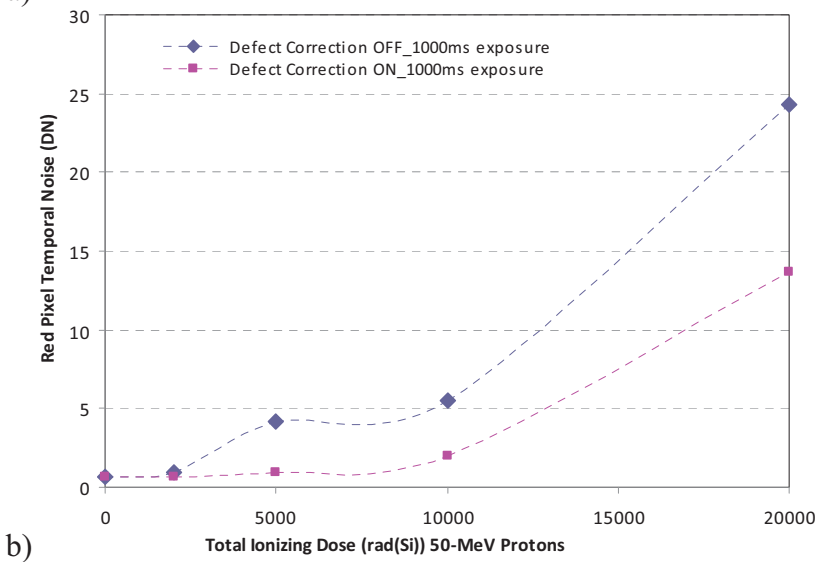


b)

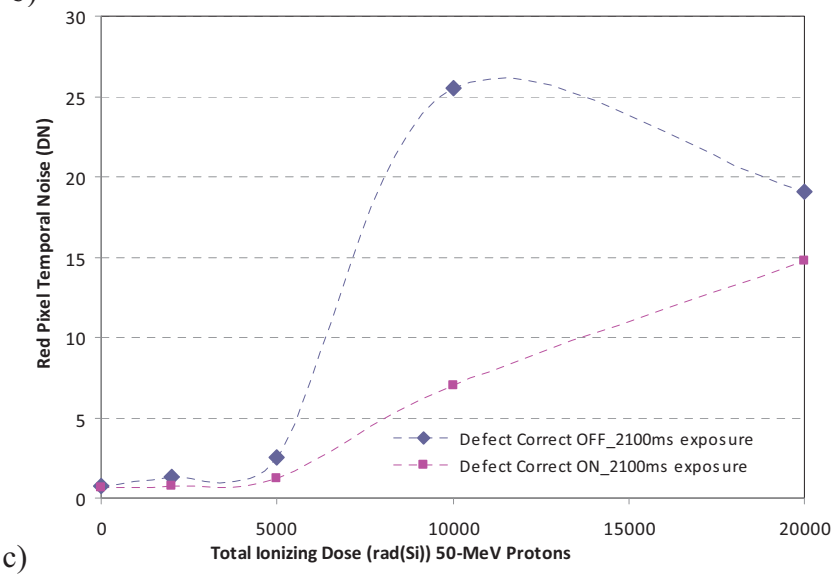


c)

**Fig. 21.** Red pixel temporal noise for samples irradiated with 50-MeV protons. Data were collected with exposure times of a) 100ms, b) 1000ms, and c) 2100ms; Gain 1.

Samples tested with Co-60 maintained very low temporal noise until 5 krad(Si) (Figure 22). At this level the powered sample showed significantly increased noise at longer exposure times (1000ms and 2100ms) until defect correction was enabled.

The loss of clear degradation trends at longer exposure times was even more pronounced in the Co-60 data than in the proton data. This is likely due to a combination of SOC functional losses, as indicated in the color bar target images taken at high TID levels, and the influence of black level conditioning on increasingly damaged pixels.

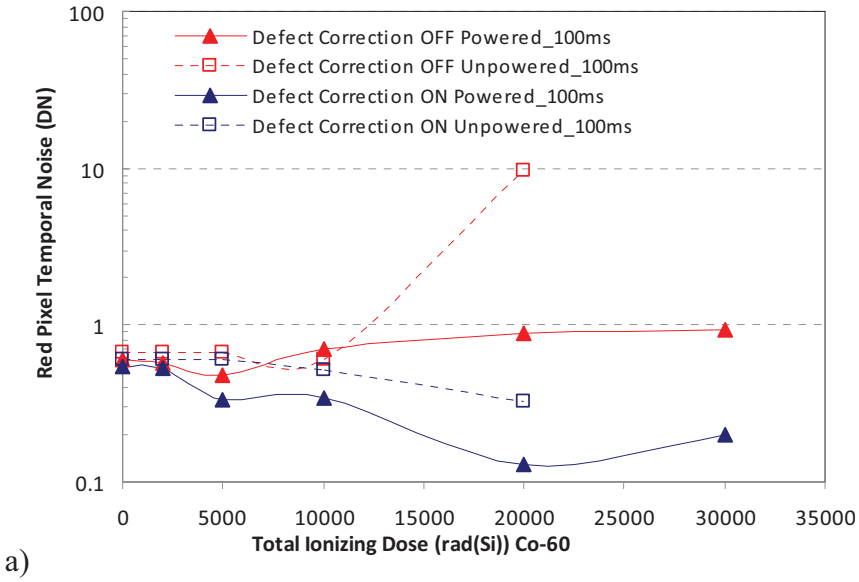


a)

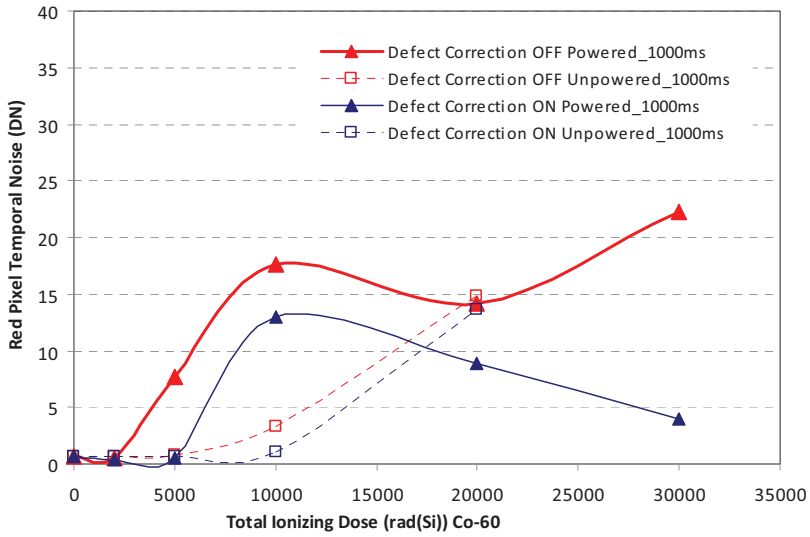


b)

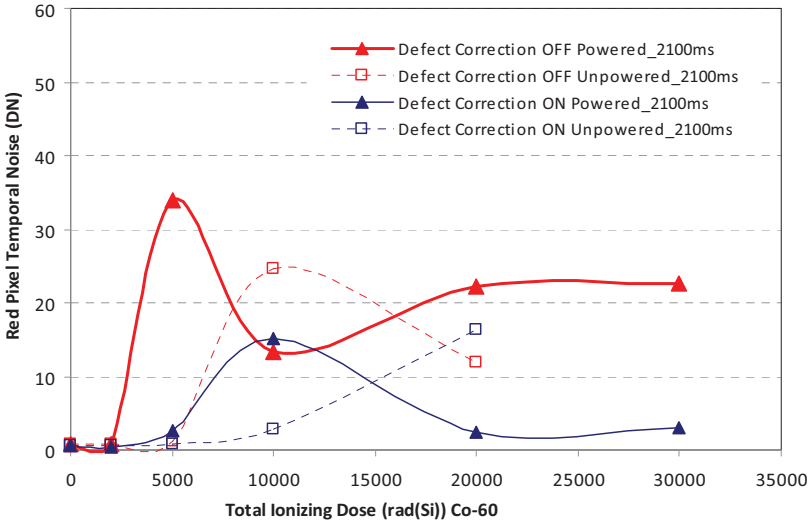


c)

**Fig. 22.** Red pixel temporal noise for samples irradiated unpowered and powered with Co-60. Data were collected with exposure times of a) 100ms, b) 1000ms, and c) 2100ms; Gain 1.

## 8.0 Conclusions

The MT9D131 System-on-a-Chip has shown excellent qualitative imaging performance following powered irradiation to 5 krad(Si) Co-60 and unbiased irradiation to 10 krad(Si) (50-MeV protons and Co-60). The on-chip defect correction function was shown to provide significant mitigation of radiation induced "hot pixels." For educational outreach or other non-scientific applications where in-flight radiation exposure predictions do not exceed these levels, the MT9131 could provide an additional commercial sensor option for camera designers. Note that for proton-dominated environments, our data is not representative of high duty cycle applications since our proton irradiations were performed with unpowered sensor samples.

As was seen with the commercial CMOS SOC evaluated under this task in FY09, OmniVision's OV3642, the integrated on-chip processing functions of such sensors makes absolute parametric characterization challenging. For science applications where absolute signal values need to be clearly understood, additional penetration into device functionality and IFP algorithms would be necessary (possibly requiring assistance from the manufacturer).

## 9.0 References


[1] Becker, H.N., Dolphin, M.D., Thorbourn, D.O., Alexander, J.W., and Salomon, P.M,, "Commercial Sensor Survey Fiscal Year 2008 Compendium Radiation Test Report," JPL Publication 08-26. October 2008.

[2] Becker, H.N., Alexander, J.W., Dolphin, M.D., Eisenman, A.R., Salomon, P.M., and Thorbourn, D.O., "Commercial Sensor Survey Fiscal Year 2009 Master Compendium Radiation Test Report," JPL Publication 09-25. October 2009.

[3] Micron Technology, Inc. "MT9D131: 1/3.2-Inch 2-Mp SOC Digital Image Sensor Features," Limited Data Sheet, Copyright © 2006 Micron Technology, Inc. http://www.aptina.com/products/soc/mt9d131c12stc/#overview. Accessed 1 June 2010. http://www.theimagingsource.com/downloads/mt9d131.en_US.pdf. Accessed 25 August 2010.

[4] Aptina™ Imaging. "Aptina MT9D131 Image Sensor Headboard." Rev.B 8/10 EN, Copyright © 2005 Aptina Imaging Corporation. http://www.aptina.com/support/documentation.jsp?t=0&q=105. Accessed 24 August 2010.

[5] Pickel, J.C., Kalma, A.H., Hopkinson, G.R., and Marshall, C.J., "Radiation Effects on Photonic Imagers – A Historical Perspective," *IEEE Trans. Nucl. Sci*., vol. 50, no. 3, pp. 671–688, June 2003.

[6] Janesick, J.R. Scientific Charge-Coupled Devices. Bellingham, WA: SPIE Press, 2001. pp. 101-105.

## Appendix 1 – Sensor Selection Criteria [1]

The survey for candidate test sensors focused primarily on low-cost (from a few tens of dollars to a few hundred dollars per sensor), low-power, commercial CMOS sensor products, such as those used in cell phones, webcams, or consumer-grade digital still cameras. Only inexpensive, commercial imagers with potential for use in low-duty-cycle space exploration applications were considered; the task does not address high-cost science grade imagers or hardened technologies. Charge coupled devices (CCDs) are typically at least an order of magnitude higher in cost than their CMOS counterparts, and they also require more complicated support circuitry to evaluate. Therefore, we did not put emphasis on CCDs in the FY07 candidate survey. Cameras for outreach programs or low-cost surveys should be relatively inexpensive to both build and host on a spacecraft and, ideally, they should be small in size. Limitations on telemetry bandwidths, power, mass, and requirements on spacecraft real estate are key considerations that helped to guide the choice of which sensors to target.

Small bandwidths suggest that large arrays with as many as 14 Megapixels (Mpixel) may not be practical for the applications we are considering. In fact, many space missions have successfully used 0.5- to 2-Mpixel monochromatic CCD cameras with filter wheels to provide excellent images. However, filter wheels add expense and also significant mass, so the choice of color detectors with 1 to 5 Mpixel (which can provide similar color resolution) presents a reasonable compromise.

Optics are an additional camera cost driver, so it is important to keep them small when designing an inexpensive camera. Common small detector optical formats are 1/4, 1/3, 1/2.5, and 1/2 inch. For a fixed set of optics, decreasing the pixel size can increase resolution, but it also decreases the amount of signal charge that an individual pixel can collect, which reduces dynamic range. Note that the photosensitive active area of pixels, the portion of which is described as "fill factor," is further reduced in CMOS sensors due to the presence of circuitry within the individual pixels. This problem is mitigated in some sensor designs by the use of microlenses or by backside illuminated sensors. Microlenses are small lenses that are placed directly on top of the pixels to focus light into the photosensitive region of the pixel.

Our trades led us to consider pixels widths between ~2 and 8 microns (μm), array sizes of ~1 to 6 Mpixel, color arrays, and 1/4- to 1/2-inch optical formats. Candidates also had to be available as packaged parts, not bare die.

The major criteria for selection were:

(1) Low cost.
(2) Sensor format, geared toward suitability for the applications mentioned above.
(3) **Relative ease of evaluation** (with the goal to minimize test development costs): A manufacturer-endorsed evaluation kit had to be available for the sensor line, and the kit was required to have the potential to easily adapt to the logistics of incremental dose testing on multiple samples. Our requirements also included the ability of the evaluation kit to produce RAW format images and provide direct control over a few select parameters, such as integration time.